Proceedings of the 1999 IEEE Canadian Conference on Electrical and Computer Engineering
Shaw Conference Center, Edmonton, Alberta, Canada May 9-12 1999

Fast Carrier Recovery for Burst-Mode Coherent Demodulation Using Feedforward Phase and Frequency Estimation Techniques

Nestor Caouras, Robert Morawski, Tho Le-Ngoc

Department of Electrical and Computer Engineering
Concordia University, 1455 de Maisonneuve Blvd. West
Montreal, Quebec, Canada H3G 1M8
nestor, robert, tho@ece.concordia.ca

Abstract

This paper describes novel feedforward data-aided digital estimation algorithms for determining carrier phase and frequency offsets independently in a burst-mode linear channel environment corrupted by additive white Gaussian noise. The techniques are applicable to linear modulation schemes (M-PSK, M-QAM) and based on oversampling of a known preamble. The estimators' performance is analyzed, simulated and verified experimentally for QPSK/OQPSK systems. Experimental results demonstrate that the techniques provide a fast synchronization using a short preamble and low complexity.

1 Introduction

Carrier recovery (CR) algorithms based on feedback and feedforward structures operating on a single sample per symbol have been widely used. Feedback schemes usually perform well in tracking environments, but may suffer from hangup problems during acquisition [1]. On the other hand, feedforward schemes avoid some of the problems usually associated with feedback loops and are very well suited for burst-mode systems due to their short acquisition time. However, digital implementation complexity associated with maximum-likelihood (ML) or approximations to ML estimators for carrier phase and frequency offsets can be quite costly if high performance is required [2-3].

This paper describes novel feedforward data-aided (DA) digital estimation algorithms for determining carrier phase and frequency offsets independently in a burst-mode linear channel environment corrupted by additive white Gaussian noise (AWGN). The proposed sub-optimum techniques attempt to balance hardware complexity and performance by oversampling and processing the received data sequence at a rate higher than the symbol rate, which is the main difference from previous techniques. Although the algorithms are applied to linear modulation formats such as M-ary phase shift keying (M-PSK) and M-ary quadrature amplitude modulation (M-QAM), only the analysis pertaining to M-PSK is presented with QPSK and Offset-QPSK (OQPSK) serving as illustrative examples. After a brief description of the system model and the Cramer-Rao lower bounds, the algorithms are described and their performance is evaluated. Implementation issues are briefly discussed.

2 Background

2.1 Signal Model

The baseband samples of an M-PSK signal can be represented as

$$z_n = a_n \exp[j(2\pi f_{off} T_{sa} n + \theta)] + v_n, \quad n = 0,1,\ldots,N-1 \quad (1)$$

where f_{off} is the carrier frequency offset we wish to estimate in Hertz, $1/T_{sa}$ is the sampling frequency equal to an integer multiple K of the symbol rate $1/T_{sym}$, n is the sample index, N is the number of samples in the observation window, a_n are the symbols of energy E_s taken from the M-PSK alphabet $\{\exp[j((2i+1)\pi/M], i = 0,1,\ldots,M-1\}$, θ is an unknown phase error uniformly distributed in $[-\pi,\pi]$, and v_n is an additive white Gaussian noise with independent in-phase (v_n^I) and quadrature (v_n^Q) components, each of zero mean and double-sided spectral density $\sigma_v^2 = N_0/2$. The pulse shaping filters, equally partitioned between transmitter and receiver, satisfy the Nyquist criterion for zero inter-symbol interference over a band-limited channel (root-raised cosine (RRC) filters are assumed with a 50% rolloff).

The frequency offset f_{off} may be rewritten more conveniently as an incremental phase error normalized to the sampling rate, $\Omega = 2\pi f_{off} T_{sa}$. The phase and frequency offsets are assumed unknown but non-random parameters, and constant for the duration of the burst. The symbol timing is assumed perfectly known at the receiver [4].

0-7803-5579-2/99/$10.00 © 1999 IEEE

2.2 *Cramer-Rao Lower Bound*

Before presenting the algorithms, this section determines the Cramer-Rao lower bound (CRLB) – a lower limit on the estimators' variance that cannot be beaten by any unbiased estimator. The CRLB for the estimate $\hat{\theta}$ is easily determined as [5]

$$\mathrm{var}(\hat{\theta}) \geq \frac{1}{2N(E_s/N_0)} \tag{2}$$

while that for the estimate $\hat{\Omega}$ is

$$\mathrm{var}(\hat{\Omega}) \geq \frac{6}{N(N^2-1)(E_s/N_0)} \tag{3}$$

where the symbol-energy-to-noise ratio is $E_s/N_0 = E_s/(2\sigma_v^2) = (E_b/N_0)\log_2 M$ and E_b is the bit energy.

3 Phase Offset Estimation

3.1 *Description of Phase Estimator*

The phase estimator proposed in this paper is derived from the first order statistic of the samples:

$$\begin{aligned} E[z_n] &= E\left\{\sqrt{E_s}\exp(j\Omega n+\theta) + v_n^I + jv_n^Q\right\} \\ &= \sqrt{E_s}\exp(j\Omega n+\theta) \end{aligned} \tag{4}$$

where the noise terms are zero-mean by definition. If a large number of samples is used, then the random process may be considered ergodic and the expectation in (4) can be approximated by its time average. The phase error estimator is now derived from the time-average equation given by

$$\begin{aligned} \lambda_l &= \frac{1}{N}\sum_{n=l}^{l+N-1} z_n = \frac{1}{N}\sum_{n=l}^{l+N-1}\left\{\sqrt{E_s}\exp(j\Omega n+\theta) + v_n^I + v_n^Q\right\} \\ &= \frac{1}{N}\sum_{n=l}^{l+N-1}\sqrt{E_s}\exp(j\Omega n+\theta) \end{aligned} \tag{5}$$

The phase argument $\hat{\theta}$ of λ_l in (5) is easily found to be the total phase error estimate at the middle of the observation window of N samples, where N is odd-valued. Clearly from (6), if the frequency error is zero, then the estimated phase error $\hat{\theta}$ corresponds to the fixed phase error θ. The estimation range in this case is bounded by $|\hat{\theta}| < \pi$.

$$\hat{\theta} = \arctan\left\{\frac{\mathrm{Im}\left\{\frac{1}{N}\sum_{n=l}^{l+N-1} z_n\right\}}{\mathrm{Re}\left\{\frac{1}{N}\sum_{n=l}^{l+N-1} z_n\right\}}\right\} = \theta + \Omega\left[l + \frac{(N-1)}{2}\right] \tag{6}$$

Equation (6) is a result of ML estimation theory and is very similar to the Viterbi and Viterbi (V&V) algorithm except that $M = 1$ here for DA operation and that the non-linearity used in V&V can be set to unity [6]. In addition, the sampling rate is higher here than in the V&V technique. Since (6) results from ML estimation theory, its variance is expected to approach the CRLB [7].

3.2 *Performance of Phase Estimator*

The performance of $\hat{\theta}$ was evaluated by simulation in burst mode QPSK and OQPSK using the signal model developed in section 2. Fig. 1 graphs the mean of $\hat{\theta}$ versus the true phase offset for the case of zero frequency error, $N = 64$, $L = K = 16$, and $E_b/N_0 = 5$dB. From the figure, the estimator assesses on the average the true phase error for virtually the entire range $[-\pi,\pi]$ except where the phase folds over owing to the modulus 2π property of $\hat{\theta}$. Since the mean of $\hat{\theta}$ equals the parameter to be estimated, $\hat{\theta}$ is unbiased in the range $[-\pi,\pi]$. The chosen window size is even. The reason for this is explained in the following paragraph.

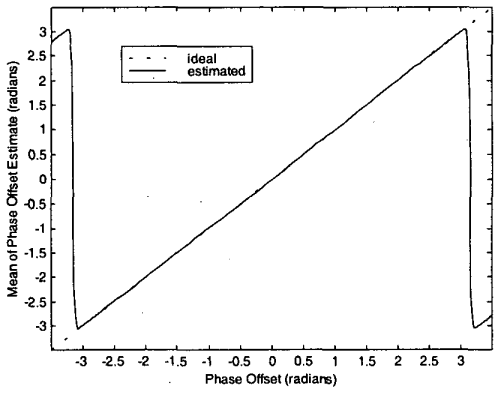

Fig. 1. Mean of $\hat{\theta}$ versus True Phase Error.

The variance of $\hat{\theta}$ is plotted in Fig. 2 for even observation windows, zero frequency error, and QPSK modulation (OQPSK yielded a similar performance since the same linear channel was used). Although (6) was originally designed for odd window sizes, its performance was evaluated for odd and even N. The results for even window sizes followed the natural interpolation between the performance points for odd windows, rendering this estimator very attractive for digital implementation.

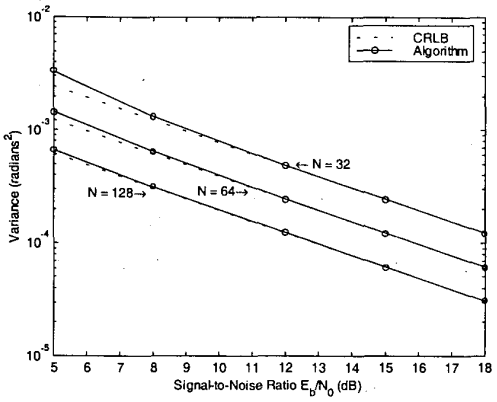

Fig. 2. Variance of $\hat{\theta}$ versus E_b/N_0.

For the DA case, the variance of $\hat{\theta}$ is very close to the CRLB, especially for moderate to high E_b/N_0, indicating that $\hat{\theta}$ can achieve the lower performance bound of an efficient estimator, which is very desirable. This is a direct result of ML estimation principles.

The probability density function of the random noise's phase is the only parameter affecting the variance of the phase estimate and follows a similar distribution as the one derived in [8-9] for the non-data-aided case operating at the symbol rate. Therefore, the variance of $\hat{\theta}$ can be easily obtained by numerical integration for the DA mode using the sampling rate instead of the symbol rate. The interested reader is referred to [8-9] for the details.

The proposed phase offset estimator is computationally very efficient since it requires little hardware for its implementation. The algorithm uses $2N$-2 real additions, one scaling function easily reduced to a shift operation if N is an integer power of 2, and a read-only memory (ROM) for storing the arctangent values.

In order to verify the concepts put forth in the previous section, the phase estimator was tested experimentally with OQPSK. The bit-error-rate (BER) curve is shown in Fig. 3 for coherent OQPSK using the phase estimator and compared against the ideal case.

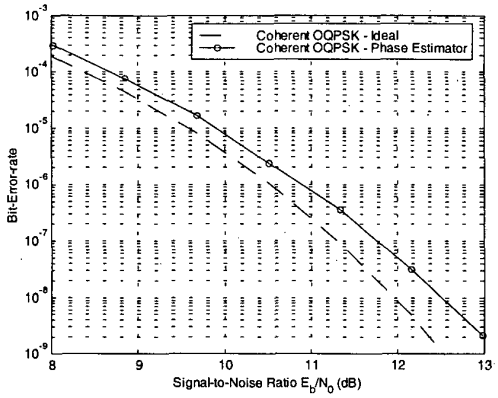

Fig. 3. Bit-Error Rate for OQPSK Modem.

The phase recovery system using $\hat{\theta}$ and four preamble symbols is about 0.4dB worse than the theoretical BER, indicating that the carrier phase error is quickly and accurately identified.

4 Frequency Offset Estimation

4.1 Description of Frequency Estimator

Based on the ergodic principle, $\hat{\Omega}$ is found by first calculating the time average of samples separated by a fixed correlation distance L over a window of N samples:

$$r(L) = E[z_n z_{n-L}^*] = \frac{1}{N}\sum_{n=l+L}^{l+N+L-1} z_n z_{n-L}^* \qquad (7)$$

where the asterisk denotes complex conjugate. Note that estimation cannot begin until L samples have been stored in memory, therefore requiring a total of N+L samples. Fortunately, this technique operates independently of $\hat{\theta}$ so that the same first N observations are used for both algorithms, with only L additional samples for the estimation of Ω.

Substituting z_n of (1) into $r(L)$ of (7) yields

$$r(L) = \frac{1}{N}\sum_{n=l+L}^{l+N+L-1}\{E_s \exp(j\Omega L)\} + r_v^I(L) + r_v^Q(L) \qquad (8)$$

where $r_v^I(L)$ and $r_v^Q(L)$ are the autocorrelation functions of the in-phase and quadrature noise components, respectively. After some straightforward manipulations, (8) leads to

$$\hat{\Omega} = \frac{1}{L}\arg[r(L)]$$
$$= \frac{1}{L}\arctan\left\{\frac{E_s \sin(\Omega L)}{E_s \cos(\Omega L) + r_v^I(L) + r_v^Q(L)}\right\} \quad (9)$$

The effect of $r_v^I(L)$ and $r_v^Q(L)$ on $\hat{\Omega}$ is easily removed by selecting L as an integer multiple of K, since the noise samples at the output of the matched filter are Gaussian random variables with autocorrelation given by

$$r_v^I(L) = r_v^Q(L) = \frac{N_0}{2K} sinc\left(\frac{\pi L}{K}\right)$$
$$= \begin{cases} 0, & L = pK,\ p = 0,1,2,... \\ \neq 0, & otherwise \end{cases} \quad (10).$$

Observe that noise samples are highly correlated for $L < K$ while $L = 0$ is of trivial interest. Choosing $L = pK$, where p is a positive integer, simplifies the expression in (9) to

$$\hat{\Omega} = \frac{1}{pK}\arctan\left\{\frac{\mathrm{Im}\left\{\frac{1}{N}\sum_{n=l+L}^{l+N+L-1} z_n z_{n-pK}^*\right\}}{\mathrm{Re}\left\{\frac{1}{N}\sum_{n=l+L}^{l+N+L-1} z_n z_{n-pK}^*\right\}}\right\}$$
$$= \frac{1}{pK}\arctan\left\{\frac{\sin(\Omega pK)}{\cos(\Omega pK)}\right\} = \Omega \quad (11).$$

The estimation range of $\hat{\Omega}$ is restricted to $|\hat{\Omega}| < \pi / L$.

4.2 *Performance of Frequency Estimator*

This section presents simulation results for the mean and variance of $\hat{\Omega}$. Fig. 4 plots the mean of $\hat{\Omega}$ for N = 64, $K = L$ = 16, and E_b/N_0 = 5dB for OQPSK. Setting L equal to K maximizes the estimation range of $\hat{\Omega}$ over $[-\pi,\pi]$. Indeed, the mean of $\hat{\Omega}$ is unbiased for about 90% of $[-\pi,\pi]$, outside which it suffers from modulo 2π fold-over.

The variance of $\hat{\Omega}$ (Fig. 5) does not attain the CRLB even at high E_b/N_0. However, the degradation is reduced if the estimation window N is increased, but more importantly if the correlation distance L is increased. For better performance, increasing L rather than N is preferable since L only requires additional memory, whereas N increases computational complexity. For example, when N = 64 and $L = K$ = 16 (5 symbols), the variance of $\hat{\Omega}$ is 7dB worse than the CRLB, but choosing $L = 5K$ (9 symbols) reduces this degradation to only 1dB. Selecting N = 64 and $L = K$ = 16 needs 5 preamble symbols, 4 of which can be simultaneously processed by the phase estimator.

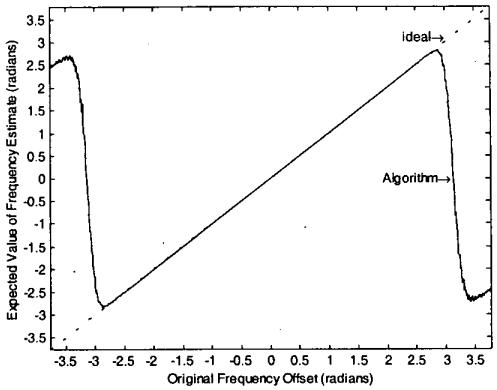

Fig. 4. Mean of $\hat{\Omega}$ versus True Frequency Offset.

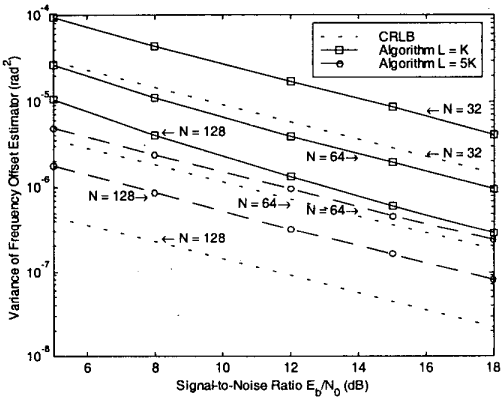

Fig. 5. Variance of $\hat{\Omega}$ versus E_b/N_0.

4.3 *Implementation of Frequency Estimator*

The frequency offset estimator requires $4N$ real products and $4N$-2 real additions. Scaling by $1/N$ follows. The argument of the accumulator averages is obtained via an arctangent ROM, a CORDIC algorithm [10], or, if Ω is known to be small, the approximation $\arctan(y/x) \approx y/x$. Final scaling by $1/L$ generates the required estimate normalized to the sampling interval. The correlation section of the circuit necessitates L unit delays. Choosing N, L and K as powers of 2 reduces the scaling operations to simple shift operations so the algorithm can be nicely implemented in hardware with low complexity.

5 Conclusions

This paper presented DA techniques for carrier phase and frequency offset estimation suitable for burst-mode communication systems. The algorithms were based on oversampling of the received data sequence. The phase estimator proved to be unbiased for almost the entire range $[-\pi,\pi]$ and approached the CRLB for moderate to high signal-to-noise ratios. The frequency estimator was unbiased for 90% of the expected estimation range but it did not achieve the CRLB. Increasing the correlation distance L by a factor of 5 for a fixed window improved its variance by 6dB and should therefore be considered in the design of a practical system. Overall, less than 10 symbols were sufficient for acceptable phase and frequency offset recovery. The feasibility of the estimators in digital hardware for OQPSK was also studied in order to demonstrate the concepts presented herein. The algorithms are equally appropriate for burst-mode M-QAM.

Acknowledgements

This work was supported by an NSERC/CRD grant with S. R. Telecom Inc. and CITR.

References

[1] F.M. Gardner, *Phaselock Techniques*, New York: John Wiley and Sons, 1979.

[2] M. Morelli, U. Mengali, "Feedforward Frequency Estimation for PSK: a Tutorial Review", *European Transactions on Telecommunications*, Vol. 9, No. 2, pp. 103-116, Mar.-Apr. 1998.

[3] H. Meyr, M. Moeneclaey, S. A. Fechtel, *Digital Communication Receivers: Synchronization, Channel Estimation and Signal Processing*, New York: John Wiley and Sons, 1998.

[4] R. Morawski, N. Caouras, Tho Le-Ngoc, "Data-Aided Fast Symbol Timing Recovery for TDMA/TDM Point-to-Multipoint Radio Communication Systems (QPSK/OQPSK)", *IEEE CCECE 1999*, Edmonton, Alberta, Canada, May 9-12 1999.

[5] D. C. Rife, R. R. Boorstyn, "Single Tone Parameter Estimation from Discrete-Time Observations", *IEEE Transactions on Information Theory*, Vol. IT-20, No. 5, pp. 591-598, Sep. 1974.

[6] A. J. Viterbi, A. M. Viterbi, "Non-Linear Estimation of PSK-Modulated Carrier Phase with Application to Burst Digital Transmission", *IEEE Transactions on Information Theory*, Vol. IT-29, No. 4, pp. 543-551, Jul. 1983.

[7] F. M. Gardner, "Demodulator Reference Recovery Techniques Suited for Digital Implementation", *Final Report to ESTEC Contract No. 6847/86/NL/DG*, Aug. 1988.

[8] R. Di Girolamo, T. Le-Ngoc, "Performance of Open-Loop Digital Frequency Estimation Techniques for Burst-Mode Transmission", *European Transactions on Telecommunications*, Vol. 7, No. 6, pp. 493-506, Nov/Dec 1996.

[9] R. Di Girolamo, T. Le-Ngoc, T., "Frequency Independent Nonlinear Feedforward Phase Estimator", *Wireless Personal Communications*, Vol. 5, No. 1, July 1997.

[10] J. Volder, "The CORDIC Trigonometric Computing Technique", *IRE Transactions on Electronics and Computers*, Vol. EC-8 , pp. 330-334, Sep. 1959.